



IMPACT ANALYSIS OF FIBER-REINFORCED COMPOSITES BASED ON ELASTO-PLASTIC CONSTITUTIVE LAW

Tae J. Kang, Kiho Joo

School of Materials Science and Engineering, Seoul National University

Keywords: Modified Drucker-Prager yield criterion, Elasto-plastic constitutive equations, Anisotropic back-stress evolution rule, 3D braided composites

Abstract

Impact analysis of 3D braided composites and laminated plane woven fabric composites was performed using the elasto-plastic constitutive law to describe the nonlinear, anisotropic and asymmetric properties of fiber-reinforced composites. As for the yield criterion, the modified Drucker-Prager yield criterion was utilized to represent the anisotropic and asymmetric properties, while the anisotropic hardening was described based on the kinematic hardening with the anisotropic evolution of the back-stress. Experiments to obtain the material parameters of the proposed constitutive law were also carried out based on uni-axial tension and compression tests for fiber-reinforced composites. Then, the proposed constitutive law was implemented into a finite element code and was verified by comparing the finite element simulation of the impact tests with experiments. In addition, impact performance of the braided composites and laminated composites was also compared with each other.

1 Introduction

Laminated composites have been used in aircraft, high performance automobiles, sporting goods industries and civil infrastructure because of their good in-plane properties and ease of handling. However, the use of the laminated composites in many engineering fields has been restricted by their poor impact resistance and low through-thickness. To overcome the drawbacks of the laminated composites, three-dimensional braided composites have been recently developed [1-4]. 3D braided composites have the ability of producing complex near-net-shape performs and this can reduce the manufacturing cost. The 3D braided composites also have higher delamination resistance and damage

tolerance for impact because of the through-thickness reinforcement.

Fiber-reinforced composites show the nonlinear behavior in stress-strain curves because of the evolution of defects such as matrix cracking, delamination and fiber breakage. To describe the nonlinear behavior of composite materials, the plasticity theory was used in this work. Because of the micro-structural changes during the deformation, the damage theory has been widely used to describe the nonlinear behavior of fiber-reinforced composites [19, 20]. However, the plasticity theory has also become popular for its simplicity [21-23]. In plasticity, the nonlinear behavior can be described only based on macroscopic uni-axial tension/compression test results without microscopic information.

In this paper, the impact performance has been evaluated based on the elasto-plastic constitutive law to describe the nonlinear behavior of laminated composites and 3D braided composites. In addition, fiber-reinforced composites show strong directional difference (anisotropy) and also the different constitutive behavior between tension and compression (asymmetry) [7, 8]. Anisotropy and asymmetry of yield criterion have been achieved by combining linear and quadratic terms of stress components [9, 10] or linear transformation of the stress deviator [11, 12].

The experimental procedure to obtain the material parameters of the proposed elasto-plastic constitutive law is also presented for laminated composites and 3D braided composites, utilizing the measured tensile and compressive stress-strain curves along various material directions.

In this paper, a plane-stress constitutive law was utilized to describe the nonlinearity and anisotropic/asymmetric properties. For the anisotropy of the fiber-reinforced composites, the initial anisotropic yielding as well as the anisotropic hardening has been considered in this work. As for the initial anisotropic yielding (and also for

asymmetry), the modified Drucker-Prager yield criterion has been used [10]. To account for the anisotropic hardening, the anisotropic back stress evolution rules based on the kinematic hardening law have been utilized [13]. The constitutive law has been incorporated into the commercial dynamic finite element code ABAQUS/Explicit using the user subroutine VUMAT [14] and impact tests have been performed to verify the simulation results. The impact properties of the braided composites are compared with plain woven laminated composites.

2 Theory

2.1 Asymmetric Orthotropic Elasticity

Different Young's moduli and Poisson's ratios were used for tension and compression.

$$\boldsymbol{\sigma} = \mathbf{C}_{T \text{ or } C}^e \boldsymbol{\varepsilon}^e \quad (1)$$

where the subscripts 'T' and 'C' mean the material properties for the tension and compression behavior respectively.

2.2 Modified Drucker-Prager Yield Criterion

The modified Drucker-Prager yield criterion was developed to describe the anisotropy and asymmetry of composite materials in the plastic deformation

$$\Phi = p[\hat{\sigma}_x^2 - \beta_{22}\hat{\sigma}_x\hat{\sigma}_y + \beta_{22}^2\hat{\sigma}_y^2 + 3\beta_{33}^2\hat{\sigma}_{xy}^2]^{1/2} + q(\hat{\sigma}_x + \kappa\hat{\sigma}_y) - \bar{\sigma}_{iso} = 0 \quad (2)$$

while, $\hat{\boldsymbol{\sigma}} = \boldsymbol{\sigma} - \boldsymbol{\alpha}$, where, $\boldsymbol{\alpha}$ is the back stress, $\bar{\sigma}_{iso}$ is the size of the yield surface, p , q , β_{22} , β_{33} and κ are material constants characterizing the anisotropic and asymmetric behavior. The modified Drucker-Prager yield criterion can describe different values of tensile yield stresses in two directions (anisotropy) and different values of tensile and compressive yield stresses (asymmetry). Also, the shear yield stress can be given independently. The five material parameters therefore can be determined from two tensile yield stresses, two compressive yield stresses, in the axial and transverse directions and the shear yield stress or the tensile yield stress along the 45 degree direction.

2.3 Hardening Rules

In the isotropic-kinematic hardening law, the effective quantities are defined considering the following modified plastic work equivalence principle; i.e.,

$$dw_{iso} = (\boldsymbol{\sigma} - \boldsymbol{\alpha}) \cdot d\boldsymbol{\varepsilon}^p = \bar{\sigma}_{iso} d\bar{\varepsilon} \quad (3)$$

where $d\boldsymbol{\varepsilon}^p$ is the plastic strain increment and $d\bar{\varepsilon}$ is the conjugate effective plastic strain increment. Here, $\bar{\sigma}_{iso}$ is obtained from the effective stress of the initial state (or the isotropic hardening case, which is relevant to the relationship, $\bar{\sigma}d\bar{\varepsilon} = \boldsymbol{\sigma} \cdot d\boldsymbol{\varepsilon}^p$) by replacing $\boldsymbol{\sigma}$ with $\boldsymbol{\sigma} - \boldsymbol{\alpha}$. Note that the effective plastic strain increment surface is stationary even for the isotropic-kinematic hardening case.

For the back stress increment, the Chaboche type back stress evolution rule [15] was used and in order to account for the directional difference of the back stress evolution for the highly anisotropic materials such as fiber-reinforced composites, the anisotropic back stress evolution rule [13] was proposed as following,

$$d\boldsymbol{\alpha} = \boldsymbol{\Gamma}_1 \cdot \frac{(\boldsymbol{\sigma} - \boldsymbol{\alpha})}{\bar{\sigma}_{iso}} d\bar{\varepsilon} - \boldsymbol{\Gamma}_2 \cdot \boldsymbol{\alpha} d\bar{\varepsilon} \quad (4)$$

where $\boldsymbol{\Gamma}_1$ and $\boldsymbol{\Gamma}_2$ are the fourth order tensors representing the anisotropic hardening behavior. For the plane stress condition, the evolution rule can be written in the matrix form

$$\begin{bmatrix} d\alpha_x \\ d\alpha_y \\ d\alpha_{xy} \end{bmatrix} = \left(\begin{bmatrix} g_{11} & g_{12} & g_{13} \\ g_{21} & g_{22} & g_{23} \\ g_{31} & g_{32} & g_{33} \end{bmatrix} \begin{bmatrix} n_x \\ n_y \\ n_{xy} \end{bmatrix} - \begin{bmatrix} h_{11} & h_{12} & h_{13} \\ h_{21} & h_{22} & h_{23} \\ h_{31} & h_{32} & h_{33} \end{bmatrix} \begin{bmatrix} \alpha_x \\ \alpha_y \\ \alpha_{xy} \end{bmatrix} \right) d\bar{\varepsilon} \quad (5)$$

where $\mathbf{n} = (\boldsymbol{\sigma} - \boldsymbol{\alpha}) / \bar{\sigma}_{iso}$ is the normal direction on the yield surface, g_{ij} and h_{ij} are the components of $\boldsymbol{\Gamma}_1$ and $\boldsymbol{\Gamma}_2$ respectively.

For the uni-axial tension test in the x direction, the following differential equation is obtained from Equation (5):

$$d\alpha_x = (g_{11}n_x - h_{11}\alpha_x)d\bar{\varepsilon} \quad (6)$$

From the associate flow rule, the in-plane components of the plastic strain increment are given as

$$d\boldsymbol{\varepsilon}^p = d\bar{\varepsilon} \mathbf{m} \quad (7)$$

where $\mathbf{m} = \partial \bar{\sigma} / \partial \hat{\boldsymbol{\sigma}}$

Equation (6) gives the following stress-strain relation, with Equation (7):

$$\sigma_x = n_x \bar{\sigma}_{iso} + \frac{g_{11} n_x}{h_{11}} \left(1 - e^{-\frac{h_{11} \varepsilon_x}{m_x}}\right) \quad (8)$$

where m_x is the x component of \mathbf{m} . Then, g_{11} and h_{11} were obtained from the curve fitting of the uni-axial tensile stress-strain curve in the x direction. The other two components for each matrix in Equation (8) are determined from the parallelism of $\boldsymbol{\alpha}$ and $\boldsymbol{\sigma}$. In this case, $g_{21} = h_{21} = g_{31} = h_{31} = 0$. For cases of simple tension in the y direction and pure shear tests, the similar formulations are possible [11]. Note that the pure kinematic hardening is considered here; i.e., $\bar{\sigma}_{iso}$ remains constant during the plastic deformation. Also, the associate flow rule was used for the in-plane components of the plastic strain increment while the non-trivial out-of-plane component of plastic strain increment is given from the incompressibility; i.e.,

$$d\varepsilon_z^p = -d\varepsilon_x^p - d\varepsilon_y^p \quad (9)$$

2.4 Numerical implementation

The developed elastic-plastic constitutive law was implemented into the general purpose finite element program ABAQUS/Explicit using the material user subroutine VUMAT [14]. To update the stress increment which involves solving a non-linear equation, the Newton-Raphson method based on the incremental deformation theory was utilized [16].

Based on the constitutive law developed here, the stress update scheme is outlined using the predictor-corrector method based on the Newton-Raphson method. The updated stress is initially assumed to be elastic for a given discrete strain increment $\Delta\varepsilon$. Therefore,

$$\boldsymbol{\sigma}_{n+1}^T = \boldsymbol{\sigma}_n + \mathbf{C} \cdot \Delta\varepsilon \quad (10)$$

where the superscript ‘ T ’ stands for a trial state and the subscript denotes the process time step. Also, the trial plastic quantities are preserved as the previous values,

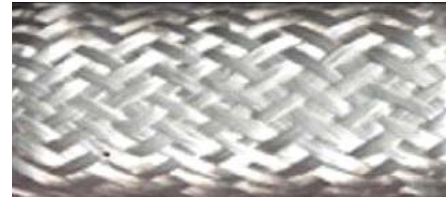
$$\bar{\varepsilon}_{n+1}^T = \bar{\varepsilon}_n \quad \text{and} \quad \boldsymbol{\alpha}_{n+1}^T = \boldsymbol{\alpha}_n \quad (11)$$

If the following yield condition is satisfied with the trial values for a prescribed elastic tolerance Tol^e for each active surface,

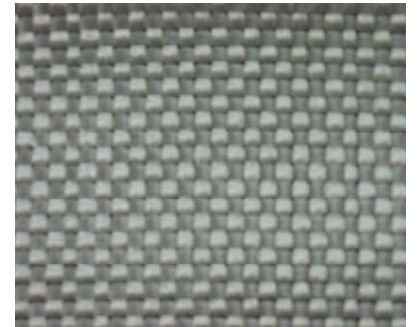
$$\Phi = \bar{\sigma}(\boldsymbol{\sigma}_{n+1}^T - \boldsymbol{\alpha}_{n+1}^T) - \bar{\sigma}_{iso} < Tol^e \quad (12)$$

the process at the step $n+1$ is considered elastic. If the above condition on yielding is violated ($\Phi > Tol^e$), the step is considered elasto-plastic and the trial elastic stress state is taken as an initial value for the solution of the plastic corrector problem until the yield condition is satisfied during the iteration.

3 Material Characterization



(a) braided



(b) laminated

Fig. 1. Preforms of (a) 3D braided composites and (b) Laminated plane woven composites

3.1 Material Preparation

The preform of the 3D braided fiber reinforced composites was fabricated using the 3D circular braiding machine with 2014 carriers and 104 pistons and by 4 step cycle movements[13,14] as shown in Figure 1 (a). The preform of the laminated plane woven fabric composites which best fit the volume fraction and thickness of the braided composites, was made by laminating seven layers of the plane glass-fiber woven fabrics with the same directional alignment as shown in Figure 1 (b). For the composite preform fabricated, RTM (Resin Transfer Molding) process was performed using the epoxy resin as matrix. After 10 hours’ injection of the epoxy resin into the RTM cast and curing in the oven at 130°C for 120 minutes, the 3D braided fiber

reinforced composites and the laminated plane woven fabric composites were prepared.

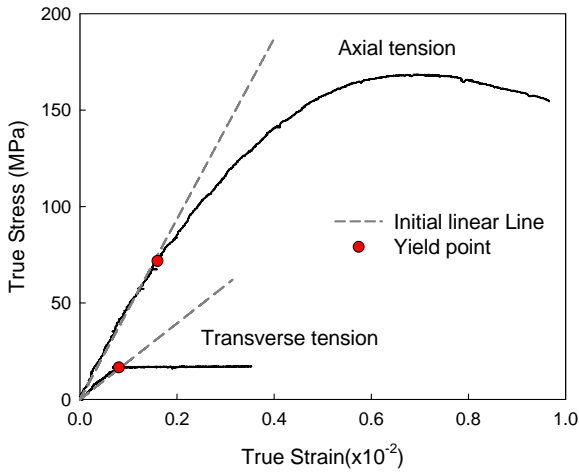


Fig. 2. Tension test results of braided composites

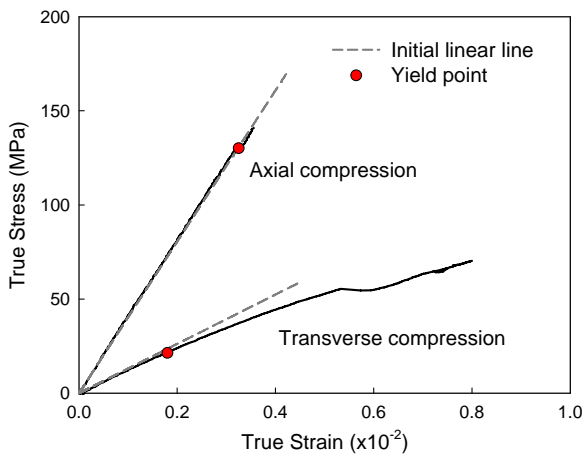


Fig. 3. Compression test results of braided composites

3.2 Elastic Properties

The tensile and compressive tests of braided composites and laminated composites were carried out by the standard procedures, ASTM D3039-76 and ASTM D3410-87 using the 10-ton tensile and compression test machine Instron 8516 system. The measured true stress-strain curves of tension and compression tests are shown in Figures 2-4 for braided and laminated composites, respectively.

The pure shear tests of composite materials were carried out by the standard procedures, ASTM D5379-93 using the Iosipescu shear test fixture. In this test, the specimen is inserted into the fixture with the V shaped notch located along the center line and fixed with thumb-screws. The shear modulus could be also determined from the 45 degree tension test.

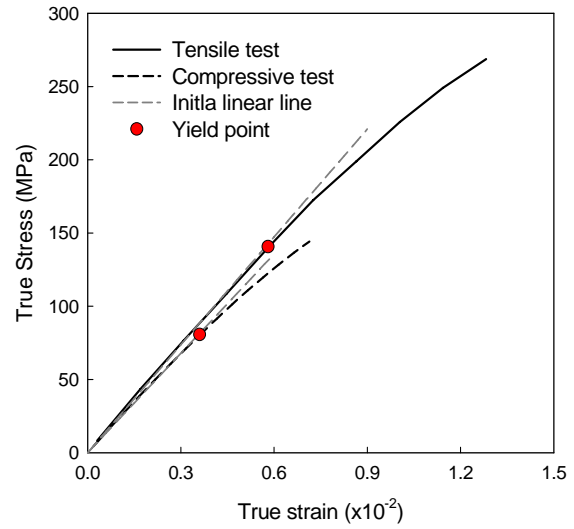


Fig. 4. Tension and compression test results of laminated composites

Table 1. The elastic constants of braided composites and laminated composites

	Braided	Laminated	Explanation
E_x^T (GPa)	46.81	24.55	tensile modulus in x-dir
E_y^T (GPa)	19.74	24.55	tensile modulus in y-dir
E_x^C (GPa)	37.74	22.61	compressive modulus in x-dir
E_y^C (GPa)	13.10	22.61	compressive modulus in y-dir
G (GPa)	11.10	5.30	shear modulus (experiment)
	13.85	2.02	shear modulus (calculation)
ν_x	0.18 ^a	0.17 ^b	Poisson's ratio

Table 2. Measured yield stresses of braided composites and laminated composites

	Braided	Laminated	Explanation
σ_x^T (GPa)	71.8	140.8	Tensile yield stress in x-dir
σ_y^T (GPa)	16.6	140.8	Tensile yield stress in y-dir
σ_x^C (GPa)	130.2	80.8	Compressive yield stress in x-dir
σ_y^C (GPa)	21.4	80.8	Compressive yield stress in y-dir
σ_1^Y (GPa)	30.8	19.9	Tensile yield stress in 45°-dir
σ_{xy}^Y (GPa)	20.3	9.8	Shear yield stress

3.3 Material Parameters for Yield Criterion

In order to account for the anisotropic and asymmetric properties of composite materials using the modified Drucker-Prager yield criterion, the five material parameters were determined from two tensile yield stresses σ_x^T , σ_y^T , two compressive yield stresses σ_x^C , σ_y^C in the x and y direction. These yield stresses were determined as the values which deviate from the linearity in the measured stress-strain curves, as marked in Figures 2-4 and listed in Table 2.

3.4 Material Parameters Hardening Laws

In order to represent the anisotropic hardening behavior using the anisotropic kinematic hardening law, the three stress-strain curves were considered after the initiation of plastic deformation: the x , y direction tension and the pure shear test curves (Tables 3 and 4). Using the material parameters obtained from the measured test data, true stress-true strain curves were re-calculated using the proposed constitutive equation as shown in Figures 5-7, which confirm good agreement with the measured data. Note that the parameters in Equation 8 were obtained from the tensile hardening curves.

Table 3: The parameters for the kinematic hardening braided composites and laminated composites

	Braided		Laminated	
	shear	45 tension	shear	45 tension
g_{11} (MPa)	110,437.6		141,787	
g_{22} (MPa)	784.05		141,787	
g_{13} (MPa)	0	-31,785.8	0	225,088
g_{23} (MPa)	0	77,867.75	0	225,088
g_{33} (MPa)	36800.04	78,651.8	70900.0	366,875
h_{11}	1066.0		903.1	
h_{22}	15.75		903.1	
h_{13}	0	-699.7	0	814.5
h_{23}	0	350.55	0	814.5
h_{33}	179.9	366.3	403.5	1,718.6

Table 4: The parameters for the isotropic hardening braided composites and laminated composites

	Braided	Laminated
$\bar{\sigma}_0$ (MPa)	71.8	140.8
a (MPa)	103.6	157.0
b	1066	903.1

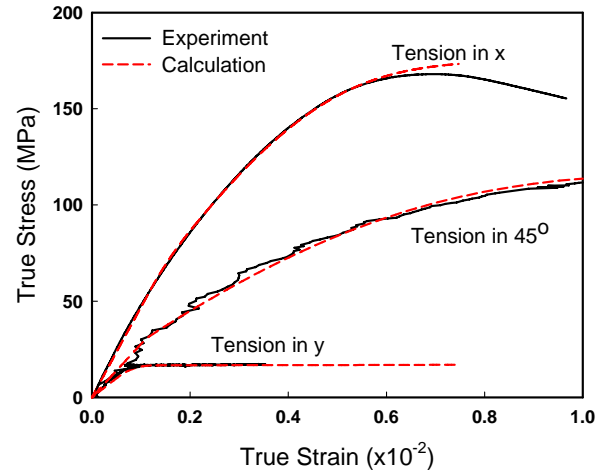


Fig. 5. Tension hardening curves of braided composites

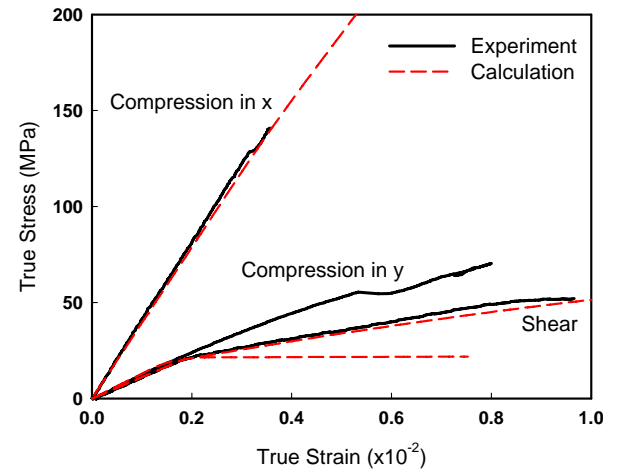


Fig. 6. Compression and shear hardening curves of braided composites

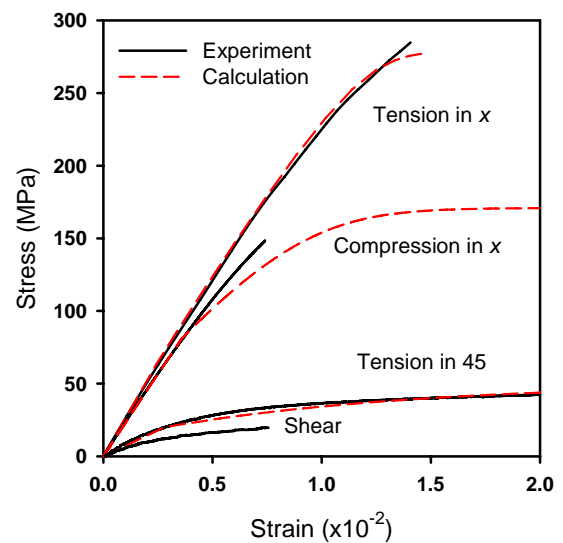


Fig. 7. Hardening curves of laminated composites

4 Impact Tests and simulations

Impact tests were performed using the impact testing system ITR-2000. The tool dimensions are 150mm(length)×150mm(width) for the rectangular die where the pneumatic clamp pressure of 500kPa is applied to hold the specimen firmly, 130mm(length)×130mm(width) for the specimen, 6.25mm for the impactor radius, 35mm for the hole radius of specimen holder and 3mm for the thickness of specimen. In the test, the specimen is initially clamped between the die and the specimen holder and then impact test is conducted using a rigid body impactor. The impact tests were carried out for two impact velocities, 2.4m/s and 3.1m/s, which correspond to the impact energy of 19J and 31J, respectively.

The load-deflection curves obtained from impact tests of braided and laminated composites are compared in Figure 8. Note that the impact instrument used for this work does not provide reasonable results after peaks so that only the data before peaks are considered. The figure shows that the peak load values of the braided composites are lower and the deflections of the impactor tip at the peaks are larger than those of laminated composites. In addition, Figure 9 shows that it takes longer for braided composites to reach the peaks. Taking these things into consideration, it can be concluded that braided composites deform larger with lower impact loads in longer period of time. The areas below the curves are similar with that the energy absorbed until the maximum peaks. This behavior is clearly seen in Figure 10 which shows the peak loads depending on the deflection and time, where 8 representative peak values for each test condition are projected to the time-deflection plane.

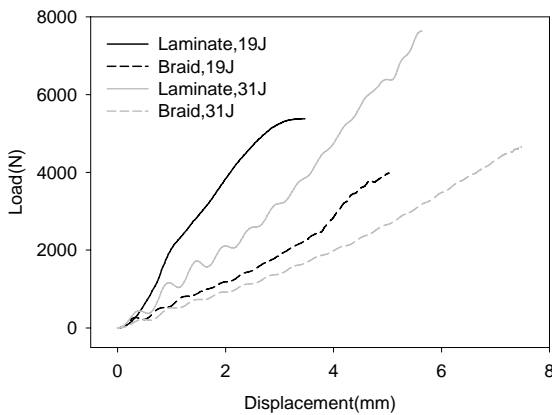


Figure 8. Typical load-displacement curves for impact tests

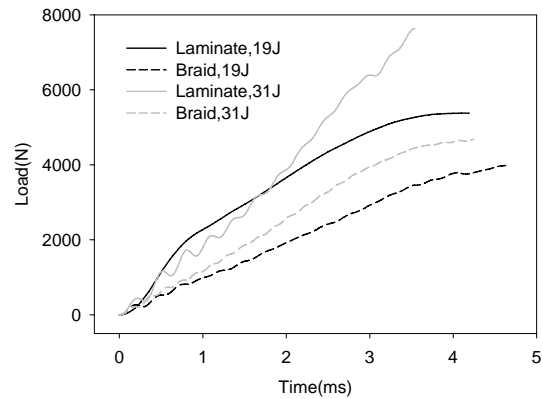


Figure 9. Typical load-time curves

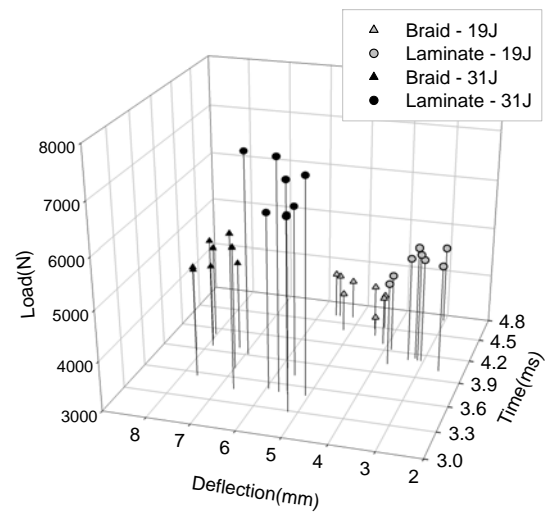


Figure 10. Peak load values of impact tests depending on deflection and time

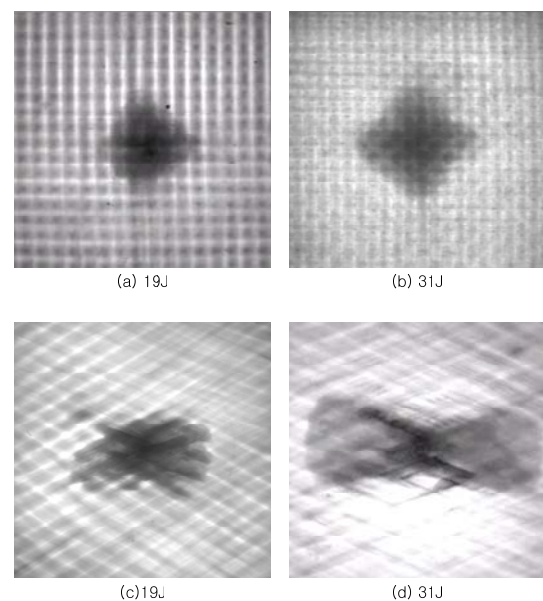


Figure 11. Images of impacted specimens for braided of impact energy (a) 19J, (b) 31J and laminated of impact energy (c) 19J, (d) 31J

The projected images taken with an equally distributed backlight are shown in Figure 11 where the images have the same specimen size and resolution and damaged parts are marked dark. The anisotropic properties of braided composites are reflected well in the figures. Damaged areas of braided composites are larger and the damage propagation profiles show stronger anisotropy than laminated composites. On the other hand, the areas for laminated composites are smaller and relatively more confined to the regions around the impacted points showing less anisotropy and negligible x - y directional dependence. Note that the directional dependence is described in x and y directions, not in the direction of the yarn path that the localized propagation along the yarn is not considered in the model.

The dominant propagation in the axial x -direction of braided composites can be explained as follows. The bending rigidity in the transverse direction is lower than the rigidity in the axial direction because the orientation angle of the yarns in braided structure is closer to the axial direction where the braiding angle for the specimen in this research was about 30° to the axial direction. Results of three point bending tests for braided composites are shown in Figure 12 [2]. The bending deformation is more likely to happen in the less resistant direction resulting large deflection finally causing dominant propagation in that direction. For the case of plain woven, the rigidities in both directions are even that the damage does not propagate in any dominant direction but rather are bounded in the surroundings of the impacted point.

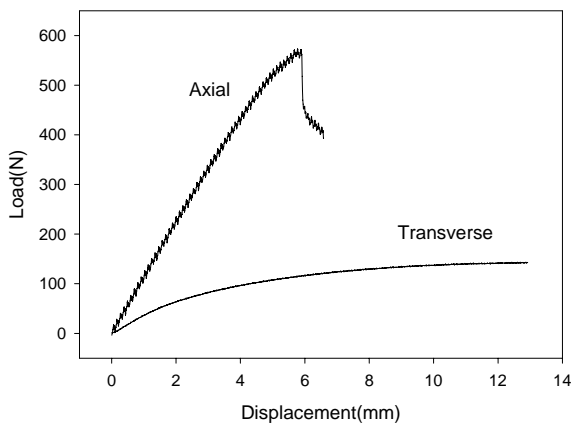


Figure 12. Load–displacement curves of three point bending tests [2]

In Figures 13 and 14, the results using asymmetric orthotropic elastic constitutive law (Case I) are compared with the experimental results. The comparison confirms that Case I significantly overestimates the stiffness, since Case I cannot account for the softness in the non-linear region of the hardening behavior.

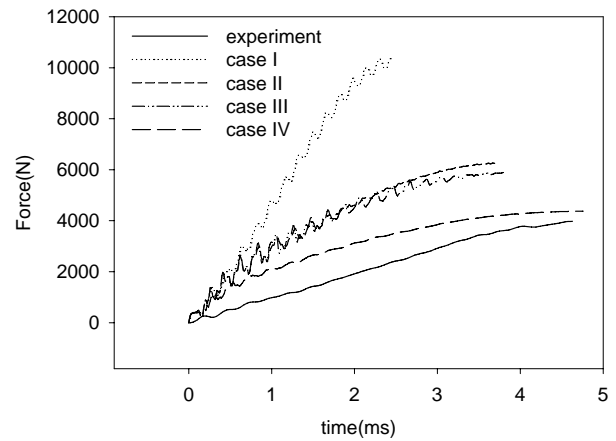


Figure 13. Time-force curves for impact tests and simulations using different yield criteria with isotropic hardening, braided, impact energy 19J

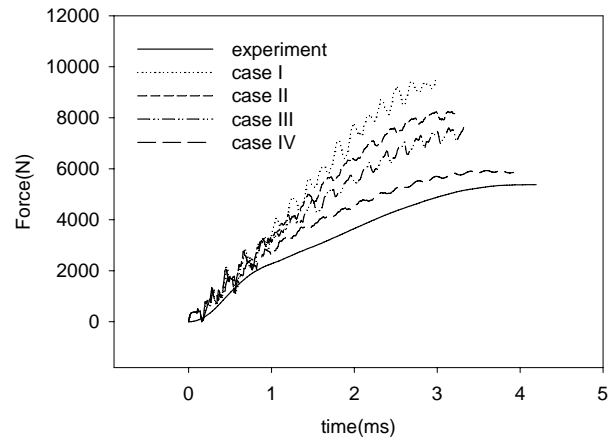


Figure 14. Time-force curves for impact tests and simulations using different yield criteria with the isotropic hardening, laminated, impact energy 19J

Figures 13 and 14 also show the comparisons of the results using the elasto-plastic constitutive law with three different yield criteria under the isotropic hardening condition: Mises yield criterion (Case II), original Drucker-Prager yield criterion (Case III) and modified Drucker-Prager yield criterion developed in this research (Case IV). The following Voce type hardening law was utilized:

$$\bar{\sigma}_{iso} = \bar{\sigma}_0 + a(1 - \exp(-b\bar{\epsilon})) \quad (2)$$

where $\bar{\sigma}_0$ is the initial yield stress in the reference direction and a and b are material parameters, which were obtained from the tensile behavior in the axial direction as shown in Table 4. Note that the results of Case II and Case III overestimated the stiffness since the Mises yield criterion does not consider both the anisotropy and asymmetry and the original Drucker-Prager yield criterion only accounts for the asymmetry. The result of Case IV is the best among all so far, since the anisotropy in the initial yielding and asymmetry are included. However, the result of Case IV still overestimated. This is because prediction of the non-linear range in the transverse and shear directions is not good enough even for Case IV since the anisotropic hardening is not accounted for. The stress-strain behavior in x direction as shown in Figures 5-7 shows much higher hardening behavior. Therefore, the behavior in the transverse and shear directions was considered as higher hardening rate for Case IV.

The modified Drucker-Prager yield criterion was used for the following comparisons. The results are compared for the proposed kinematic hardening (Case V) and the isotropic hardening (Case IV) in Figures 15 and 16. Note that as mentioned earlier, the 45 degree tensile test can be replaced with the pure shear test to account for the shear properties [17]. Therefore, the results using the 45 degree tensile test (Case VI) are also considered in this comparison. Figures 15 and 16 show that the results of Case VI are virtually the same as the results of Case V since the anisotropic hardening is properly accounted. The results also show that Cases V and VI show good agreements with the experiments since Cases V and VI properly consider the hardening differences as well as asymmetry, while Case IV does not account for the transverse and shear hardening. The data of impact energy 31J are also considered and showed similar characteristics to the data of 19J.

4 Conclusions

Impact analysis of 3D braided composites and laminated plane woven fabric composites was performed using the elasto-plastic constitutive law to describe the anisotropic and asymmetric properties. Modified Drucker-Prager yield criterion was utilized to represent the anisotropic and asymmetric

properties, while the anisotropic hardening was described based on the kinematic hardening with the anisotropic evolution of the back-stress. The model showed good agreements with the experimental data while the other models not considering asymmetry or anisotropic hardening overestimated the stiffness. The impact properties of the braided and laminated composites were compared that braided composites absorb impact energy with lower load, through longer period of time with larger deformation as propagating the stress for the larger area than the laminated composites. The constitutive model developed in this research has found to be valid that the further studies on nonlinear mechanical analysis are ongoing based on the model.

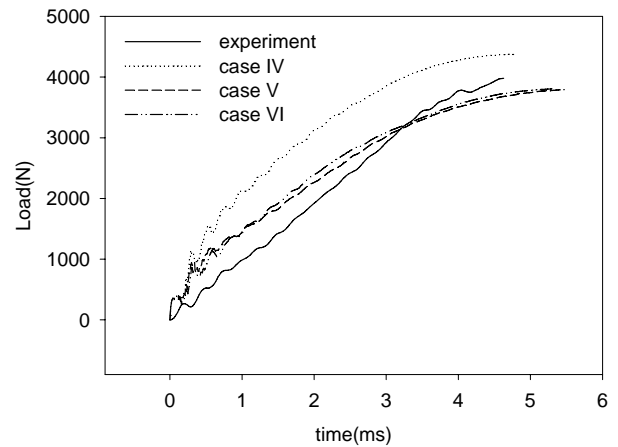


Figure 15. Time-force curves for impact tests and simulations using the isotropic hardening and anisotropic kinematic hardening laws, braided, impact energy 19J

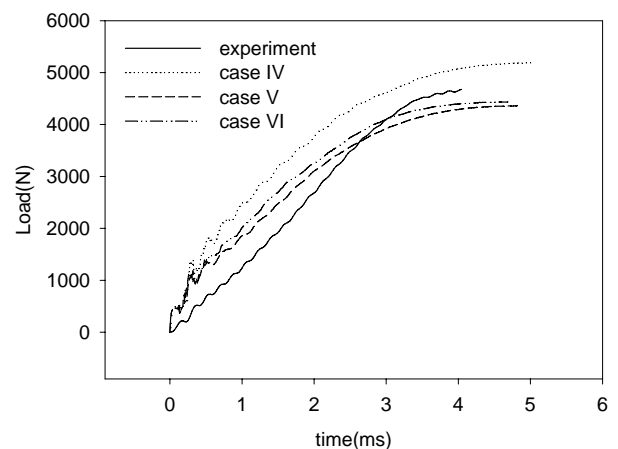


Figure 16. Time-force curves for impact tests and simulations using the isotropic hardening and anisotropic kinematic hardening laws, laminated, impact energy 19J

Acknowledgement

The authors of this paper would like to thank the Korea Science and Engineering Foundation (KOSEF) for sponsoring this research through the SRC/ERC Program of MOST/KOSEF (R11-2005-065)

References

- [1] Chung, K., Ryou H. and Lee, W. "Mechanical property of circular braided fiber composites". Proceedings of the Second International Workshop on Multi-Axial Textile Composites, Seoul National University, South Korea, pp165-183, 2004.
- [2] Ryou H., Kim J.H., Lee M.G., Kim D., Chung K., Youn J.R. and Kang T.J. "Elastic-Plastic Analysis of Three Point Bending Tests for 3D Circular Braided Glass Fiber Reinforced Composites". *Textile Science and Engineering.*, 42: 336-340, 2005
- [3] Kim, J.H., Ryou, H., Lee, M.G., Chung, K., Youn, J.R. and Kang, T.J. (accepted). Micromechanical Modeling of Fiber Reinforced Composites Based on Elasto-Plasticity and its Application for 3D Braided Glass/Kevlar Composites. *Polymer Composites.*,
- [4] Jung, K. and Kang, T.J. (accepted). Cure monitoring and internal strain measurement of 3-d hybrid braided composites using fiber Bragg grating sensor, *Journal of Composite Materials.*,
- [5] Saleeb, A.F., Wilt, T.E., Al-Zoubi, N.R. and Gendy, A.S. (2003). An anisotropic viscoelastoplastic model for composites—sensitivity analysis and parameter estimation, *Composites Part B*, 34: 21-.
- [6] Agarwal, B.D. and Broutman, L.J. (1980). *Analysis and Performance of Fiber Composites*. John Wiley & Sons, NY.
- [7] Piggot, M.R. and Harris, B. (1980). Compression strength of carbon, glass and Kevlar-49 fiber reinforced polyester resins. *J Mater Sci*, 15: 2523-2538.
- [8] Hancox, N.L. (1975). The compression strength of unidirectional carbon fiber reinforced plastic. *J Mater Sci*, 10: 234-242.
- [9] Stoughton, T.B. and Yoon, J.W. (2004). A pressure-sensitive yield criterion under a non-associated flow rule for sheet metal forming. *International Journal of Plasticity*, 20: 705-731.
- [10] Kim, J.H., Lee, M.G., Ryou, H., Lee, M.H., Chung, K., Kang, T.J. and Youn, J.R. (2005). Mechanical Analysis of 3D Braided Fiber Reinforced Composites Based on Homogenization and Elastic-Plastic Constitutive Laws, Proceedings of the 8th Esaform Conference on Material Forming, Cluj-Napoca, Romania 2005, April 27-29, 2005: 955-958.
- [11] Barlat, F., Aretz, H., Yoon, J.W., Karabin, M.E., Brem, J.C. and Dick, R.E. (2005). Linear transformation-based anisotropic yield functions, *International Journal of Plasticity*, 21: 1009-1039.
- [12] Lee, M.G., Kim, J.H., Ryou, H., Chung, K., Youn, J.R. and Kang, T. J. (2006). Numerical Implementation of Modified Coulomb-Mohr Yield Criterion for Anisotropic and Asymmetric Materials, *Fibers and Polymers*, Vol 7, No 3, 276-285.
- [13] Lee, M.G., Kim, D., Chung, K., Youn, J.R. and Kang, T.J. (2004). Combined isotropic-kinematic hardening laws with anisotropic back-stress evolution for orthotropic fiber-reinforced composites, *Polym Polym Compos*, 12: 225-234.
- [14] Hibbitt, Karlsson and Sorensen (2002). *ABAQUS User's manual*, Version 6.3.
- [15] Chaboche, J.L. (1986). Time independent constitutive theories for cyclic plasticity, *Int J Plasticity*, 2: 149-188.
- [16] Chung, K., Richmond, O. (1993). A Deformation Theory of Plasticity Based on Minimum Work Paths, *Int J Plasticity*, 9: 907-920.
- [17] Rosen, B.W. (1972). A simple procedure for experimental determination of the longitudinal shear modulus of unidirectional composites, *Journal of Composite Materials*, 6: 552-555.
- [18] Takeda, T., Shindo, Y. and Narita, F. (2004). Three-dimensional thermoelastic analysis of cracked plain weave glass/epoxy composites at cryogenic temperatures, *Composites Science and Technology*, 64: 2353-2362.
- [19] Matzenmiller, A., Lubliner, J. and Taylor, R.L., (1995). A constitutive model for anisotropic damage in fiber-composites.. *Mech Mater* , 20: 125-152.
- [20] Krajcinovic, D. (2000). Damage mechanics: accomplishments, trends and needs. *Int J Solid Struct*, 37: 267-277.
- [21] Dvorak, G.J. and Bahei-El-Din, Y.A. (1987). A bimodal plasticity theory of fibrous composite materials. *Acta Mech*, 69: 219-241.
- [22] Chen, J.K., Allahdadi, F.A. and Sun, C.T. (1987). A quadratic yield function for fiber-reinforced composites. *J Compos Mater*, 31: 788-811.
- [23] Espinosa, H.D., Dwivedi S. and Lu H.C. (2000). Modeling impact induced delamination of woven fiber reinforced composites with contact/cohesive laws.. *Comput Method Appl Mech* , 183: 259-290.